Post Hatfield rolling contact fatigue

The effect of residual stress on contact stress driven crack growth in rail

Part 1: The model

A Kapoor and DI Fletcher

November 2006

NewRail Report No. WR061106-2

NewRail | School of Mechanical & Systems Engineering | Newcastle University
NE1 7RU | UK | T+44 (0)191 222 5821 |F+44 (0)191 222 5821 | www.newrail.org

OFFICE OF RAIL REGULATION

The majority of the work reported here was undertaken at the University of Sheffield in 2003-2004, but publication was embargoed until 2006. The authors are now at Newcastle University. This issue supersedes earlier versions of the report.

Contents

1 Summary

This report presents a model for investigating the effect of residual stress in railway rails on the rate of crack growth for shallow angle rolling contact fatigue cracks. Crack growth rate results are presented for a single contact condition only, and for a single set of residual stress input conditions. Further contact conditions and residual stress distributions will be investigated and presented in a later report. Support for the crack growth rate results is presented using contour plots of stress beneath the rail-wheel contact.

The results indicate that for a shallow (30° below the surface) rolling contact fatigue crack under the conditions investigated, the crack growth rate is particularly sensitive to vertical residual stress in the rail. At crack lengths up to around 25mm predicted crack growth rates are around 1.5 those in the absence of residual stress, while at longer lengths the growth rate may be up to 100 times the rate predicted without residual stress. However, at such long crack lengths rail bending may be important, and this is not included in the current model.

This report contains revised information on the residual stress input data, and supersedes earlier versions of the report.

2 Crack growth prediction method

Calculations of crack growth rates were conducted based on the method developed by Fletcher and Beynon [1] which rely on Green's functions developed by Rooke et al. [2]. Green's functions allow the stress in an uncracked body to be used to calculate SIFs for cracks of a particular geometry. This method has the advantage that it is a quick process to calculate the required stresses, relative to the time taken to calculate stress in the cracked body using a finite element or boundary element approach. Figures 1 illustrate the Green's functions for the case of calculating mode I stress intensity factors (opening mode) from point normal forces along a crack, and mode II stress intensity factors (shear mode) from point shear forces along a crack. Further Green's functions are available for calculating the mode II SIF from normal forces, and mode I SIF from shear forces. Each type of forces leads to both types of stress intensity factor because the crack is at an angle to the surface.

Stress intensity factors are calculated by taking the product of the normal and shear stress present at each point along the cracks with the corresponding Green's function at the same position. Since force and the Green's functions are actually continuous distributions rather than a series of point values, finding the SIF requires integration of the product of force and Green's function. This is illustrated by example Equation 1, in which l is the crack length, $\sigma(n)$ is a stress, and $g(n)$ is a Green's function, and n is a position along the crack.

$$K = \frac{1}{\sqrt{\pi l}} \int_0^l \sigma(n) g(n) \mathrm{d}n \tag{1}$$

Examples of stress distributions along a crack are shown in Figure 3.

The stresses present in the material below a rail-wheel contact is shown in Figure 2. Plotting just the stresses present along the crack line produces the plots shown in Figure 3. In these plots the stresses are determined from the

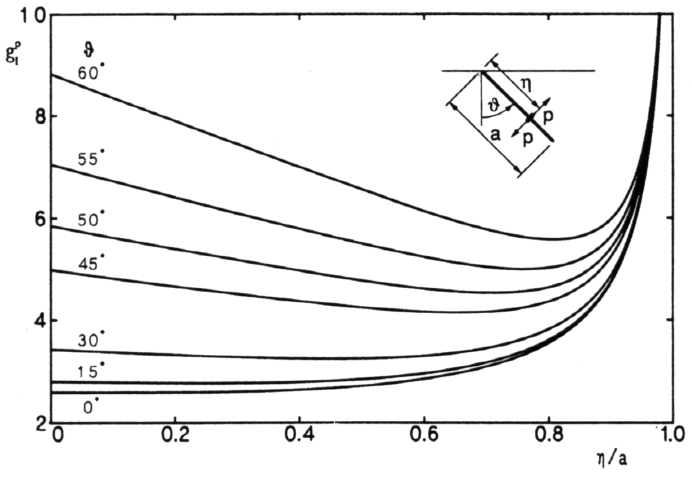

(a)

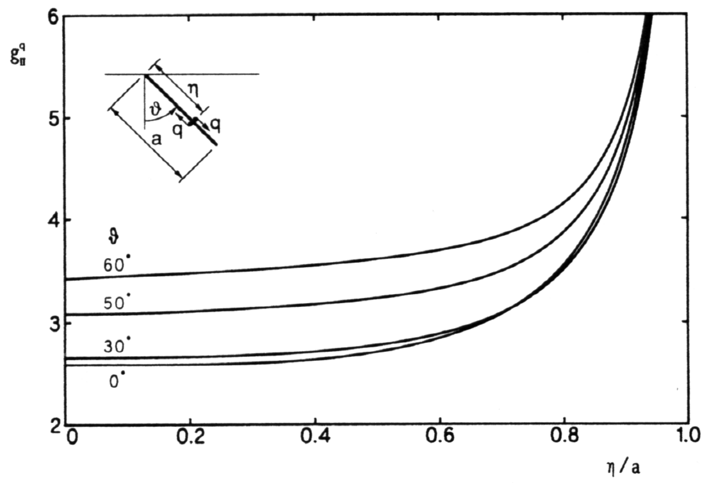

(b)

Figure 1: Crack line Green's functions due to a point force on the crack surfaces. (a) Mode I stress intensity factor generated by a normal force. (b) Mode II stress intensity factor generated by a shear force. [2]

Hertzian contact stress distribution produced by the load applied at the surface, modified to take account of crack closure and friction between the crack faces. A full description of these calculations is given by Fletcher and Beynon [1]. Briefly, stresses present in the body are resolved to give a stress normal to the crack and a shear stress parallel to the crack. Where the normal stress is compressive the crack is taken to be closed, and friction between the crack faces is taken to resist sliding of the faces, diminishing the shear stress present at those points. If the stress due to friction (product of the normal stress on the crack and the crack face friction coefficient) is sufficient to prevent sliding of the crack faces, the faces are "locked" and in that region there is no shear stress contribution to the stress intensity factor at the crack tip. Although negative normal stresses are therefore essential in the calculation of shear stresses along the crack, negative values of normal stress are assumed to make no contribution to the mode I (opening) stress intensity factor, and normal stress is set to zero for SIF calculation at points along the crack with negative normal stress. Manipulation of stresses in this way was first suggested by Kaneta and Murakami [3], and the current model produce results in good agreement with their work. The normal and shear stresses calculated in this way are defined as the "effective" stresses driving crack growth.

2.1 Previous model - without residual stress

While Green's function approaches have the advantage that they are quick relative to other methods, they have the disadvantage that they are restricted to the particular crack geometry and crack position relative to the load for which the Green's functions were developed. The earliest models developed by Fletcher and Beynon [1] using the Green's functions technique were 2d models in which a Hertzian line contact was used to calculate the stresses present in the cracked body. A more realistic representation of the rail-wheel contact is as a three dimensional contact, typically idealised as a Hertzian elliptic contact. Green's functions for a three-dimensional crack under contact loading are not currently available. However, to improve on the 2d model a hybrid model has been developed in which a three-dimensional stress field is combined with the currently available Green's functions to produce what may be referred to as a 2.5 dimensional model [4] which is explained below. While a 2.5d model cannot be expected to be as comprehensive as a full 3d finite element approach to crack growth, it is a major advance on the pure 2d model, while speed of calculation is retained. Important advantages are that:

- The use of a 3d contact patch and corresponding stress field gives a much more realistic representation of the stress within the body of a rail than did the 2d line contact approach. The intensity of the 3d stress field typically diminishes much more rapidly with distance from the contact than does the 2d stress field (for equivalent contact conditions) so crack growth rate will be lower at longer crack lengths.

- The effect of offsetting the contact position laterally from the assumed centre of the crack can be studied. This allows the simulation of, for example, contact patch re-location because of wheel-rail profile change through grinding. Already included in the 2d model was a conversion

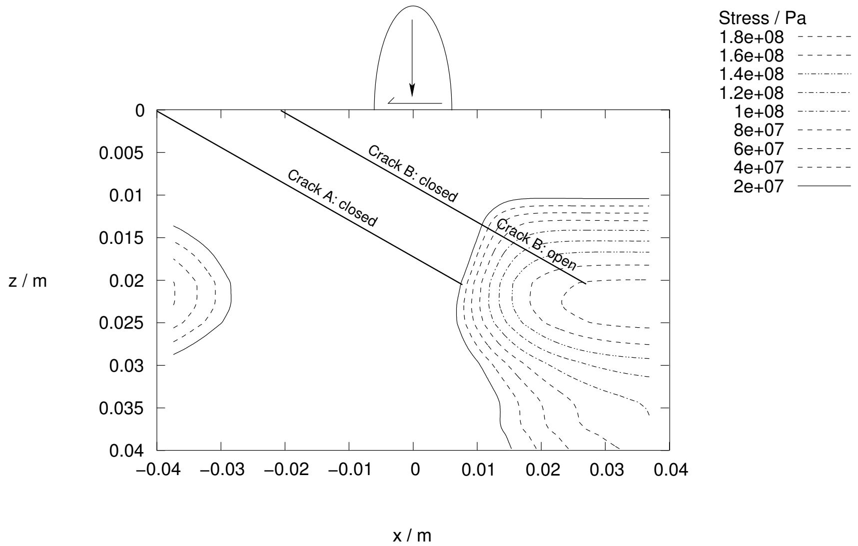

(a)

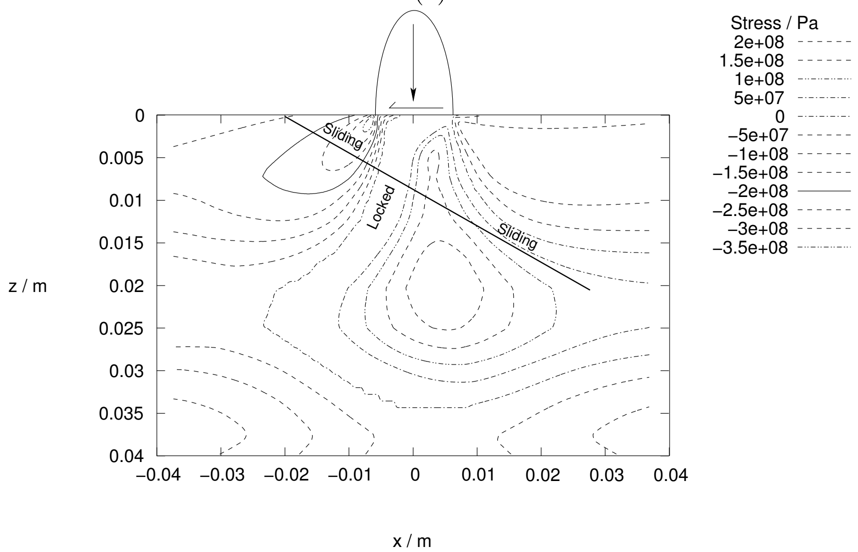

(b)

Figure 2: Contour plots of "effective" stress beneath a rail-wheel contact combined with residual stress, and modified to take account of crack closure and crack face friction. 1500MPa Hertzian line contact, surface friction coefficient of 0.18, crack face friction coefficient of 0.18, crack at 30° below the surface.(see Run 40 discussed in Section 3.2) (a) Stress resolved normal to the crack. Regions of negative stress are set to zero representing a closed crack. (b) Shear stress parallel to the crack. Stress is zero in regions of crack locking.

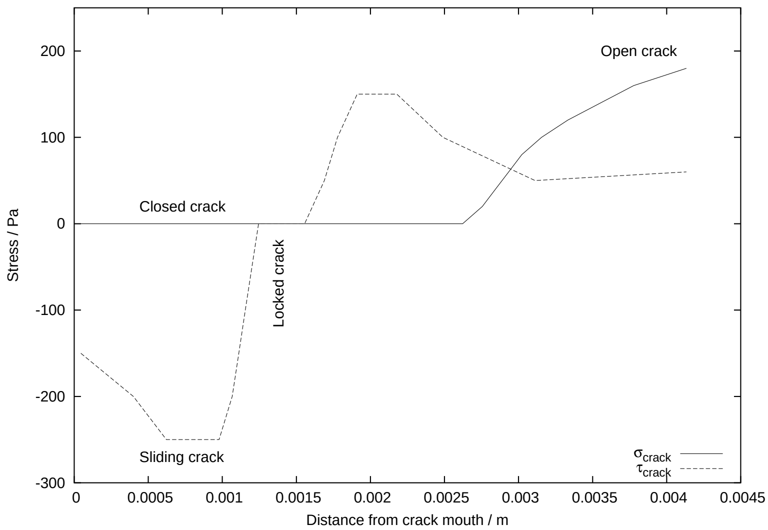

Figure 3: Examples of the "effective" stress distribution present along the cracks line for a crack at 30$\circ$ below the surface (see Run 40 discussed in Section 3.2). The solid line shows stress normal to the crack, which is set to zero in regions of negative stress because the crack is taken to be closed. The dashed line represents shear stress which may be positive or negative, but is set to zero in regions where the crack is locked.

to give results representing the effect of a line contact crossing a semi-circular crack rather than the infinitely long slot for which the Green's functions were developed. However, because the contact was a line contact of infinite length it was impossible to examine the effect of moving the contact laterally. This becomes possible when using a 3d contact, although this work has not been applied in the current project.

2.2 2.5d method

Figure 4 illustrates how the 2.5d model is related to the previously developed 2d model of crack growth. In both cases the contact is moving across a perpendicular crack of infinite width, this crack geometry being dictated by the Green's functions. To make the results more relevant to rail-wheel contact, the stress intensity factors for this infinitely wide slot can be scaled to gives values appropriate to an equivalent semi-circular crack. The ratio of geometry factors for cracks of these shapes and of equal depths was found to be 0.59 for cracks running normal to the contact surface in both uniaxial tension and pure bending. It was assumed that this factor could also be applied in the current case, even though the cracks are not normal to the contact surface.

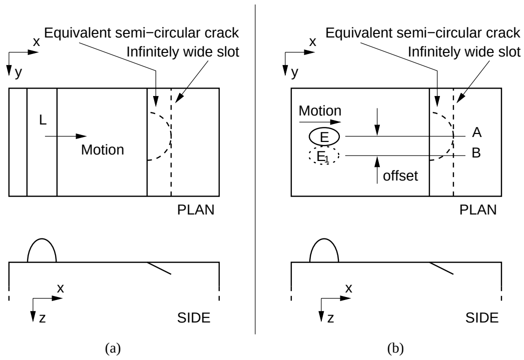

Figure 4: The 2d and 2.5d stress intensity factor calculation models. (a) A line contact L (plan view) with a semi-elliptical pressure profile (side view) crosses an infinitely wide slot, shown by the straight dashed line. An equivalent semi-circular crack can be defined with radius equal to the depth of the slot, shown with a curved dotted line. (b) The line contact is replaced by an elliptical contact E, which has a semi-elliptical pressure profile (side view), and which moves along line A. Slot and semi-circular cracks are defined as before. The contact may be offset, for example to position E1 on line B, giving a reduction in the stress driving cracks defined on line A.

As either the line or elliptical contact crosses the crack, the stresses driving crack growth are those on the xz plane (see figure 4). For a line contact these stresses are uniform for all values of y, but for an elliptical contact patch the stresses on the xz plane are dependent on the y position. Taking the origin of the coordinate system to be at the centre of the elliptical contact patch, the stress on the xz plane for $y = 0$ can be used to represent the contact passing directly over the centre of the (imaginary) semi-circular crack for which stress intensity factors are calculated. Using other values of y is equivalent to offsetting the contact by the distance y from the imagined semi-circular crack. Offsets are most conveniently specified as multiples of the contact dimension a.

It should be noted that this simple method of examining a contact offset takes no account of the crack size in determining the influence of stresses from an offset contact. For example, an offset of $2a$ for a crack of radius $0.5a$ clearly moves the contact completely away from the crack, but if the crack were of radius $2a$ it would be expected that the crack would remain significantly influenced by the contact. This is illustrated in Figure 5. For cracks which are large relative to the contact, and which have a semi-circular shape, it is likely that the crack shape may change following the offsetting of the contact, i.e. the crack would not simply grow more slowly as a semi-circular crack, but would develop most rapidly in the region that remains under the contact after it is offset, and slowly if at all in the region below the original contact centre line. Offsetting of the contact may therefore be accompanied by a reduction in the characteristic crack length which determines the crack growth rate, i.e. the length of the crack beneath the centre of the contact patch. This is shown in Figure 5. To investigate this possibility is beyond the scope of the simple treatment of contact offsets developed here, and requires a full three-dimensional approach to the problem rather than an adapted two-dimensional method.

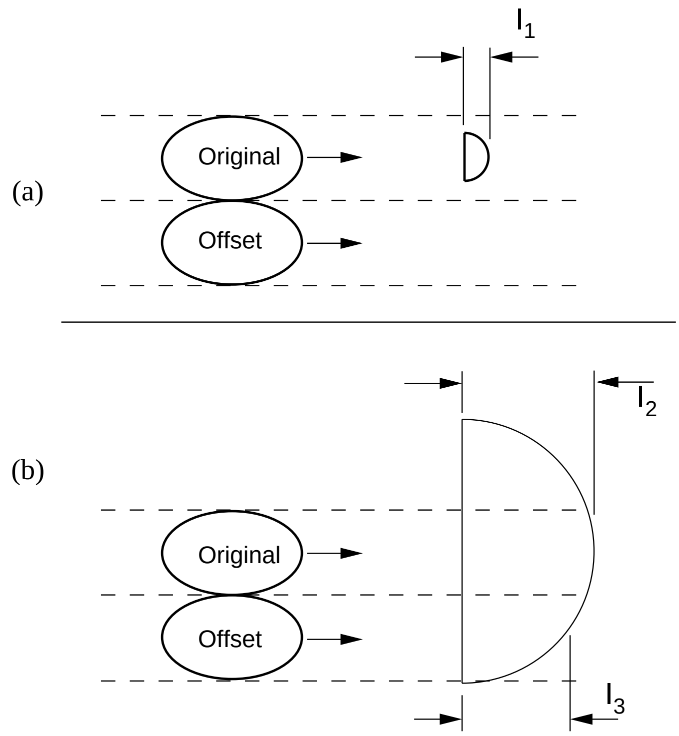

Figure 5: Offsetting a 3d contact from the centre line of a crack. (a) The original contact crosses a small crack, with a characteristic crack length (length below the centre of the contact) of l_1. After offsetting the contact, it no longer crosses the crack (b) The original contact crosses a large crack, with a characteristic length l_2. After offsetting the contact by the same amount as in (a) the contact still crosses the crack, but the characteristic length is reduced to l_3

2.2.1 Crack growth law

The crack growth law used to convert between stress intensity factors and crack growth rates for the 2.5d model is the same as was applied previously in the 2d model. It is summarised by Equations (2) and (3).

$$\frac{da}{dN} = 0.000507(\Delta K_{eq}^{3.74} - 4^{3.74}) \tag{2}$$

$$\Delta K_{eq} = \sqrt{\Delta K_I^2 + \left[\left(\frac{614}{507}\right)\Delta K_{II}^{3.21}\right]^{\frac{2}{3.74}}} \tag{3}$$

The growth rate da/dN is given in nm per cycle, and the stress intensity factors are in MPa$\sqrt{m}$. Equations [2] and [3] were developed at the University of Sheffield [5].

2.2.2 Crack face friction

Crack face friction coefficients are used together with the stress normal to the crack faces to determine the level of shear stress which when applied to the crack will be sufficient to make the crack faces slip relative to one another. The greater the proportion of the crack face that can slide, the greater will be the stress intensity factor at the crack tip. Crack face friction was implemented in the same way in the 2.5d model as it was in the 2d model.

2.3 Inclusion of residual stress in the 2d and 2.5d models.

Following calculation of the Hertzian contact stress for either a line contact (2d model) or elliptic contact (2.5d model) but prior to the multiplication and integration of the stress with the Green's function it is possible to add to the contact stress any value for residual stress present in the rail. Residual stresses vary with position, so values to be added to the contact stress are found using interpolation between available data. Currently interpolation is possible in the z (depth) direction into the rail head only, and different residual stress data sets are required to consider offsets of the contact from the rail head centre. The current model can consider vertical (z), longitudinal (x) direction stresses and zx plane shear stresses. Because of the underlying Green's functions transverse stress in the rail cannot be considered.

Addition of static residual stress to the varying contact stresses present in the rail may at first appear to make no difference to the stress intensity factor range, which is the factor controlling crack growth rate. However, because the model includes the effect of crack closure a static stress does not work simply as a mean stress, but will in fact change the proportion of the contact cycle over which the crack is closed, and thereby change the stress intensity factor range. The normal stress closing a closed crack will also be affected by the residual stresses, and this will affect the likelihood of the crack faces sliding over one another in shear. Residual stresses are added to contact stresses prior to the resolution of stress into components normal and parallel to the crack (see Section 2, and the rest of the model remains unchanged.)

3 Crack growth in presence of residual stress

3.1 Residual stress distribution

Until measured residual stress distributions for rails specific to the project become available it was decided to use values from the literature [6] to begin the investigation. The current model is able to consider the variation of residual stress with penetrated depth into the rail for a single point on the rail surface, the input data shown in Figure 6 being used throughout the work unless stated otherwise.

The model assumes that the residual stress shown in Figure 6 is applied across the entire width of the three dimensional crack in the rail. However, the available data on residual stress [6] indicates that the magnitude of these stresses varies with lateral position across the rail head. Also, the residual stress affecting crack growth will be determined by the crack orientation, which may not be (as has been assumed here) transverse across the rail. The actual crack orientation will be determined by the rail steel's response to the combination of lateral (cornering, steering) and longitudinal stress applied by the wheel. An attempt to take account of the variation of stress seen by the crack due to both its lateral width and changes in its orientation relative to the longitudinal axis of the rail is to consider both standard and reversed residual shear stresses acting on the crack, i.e. runs were completed with both the standard residual shear stress values, and with these values multiplied by -1.

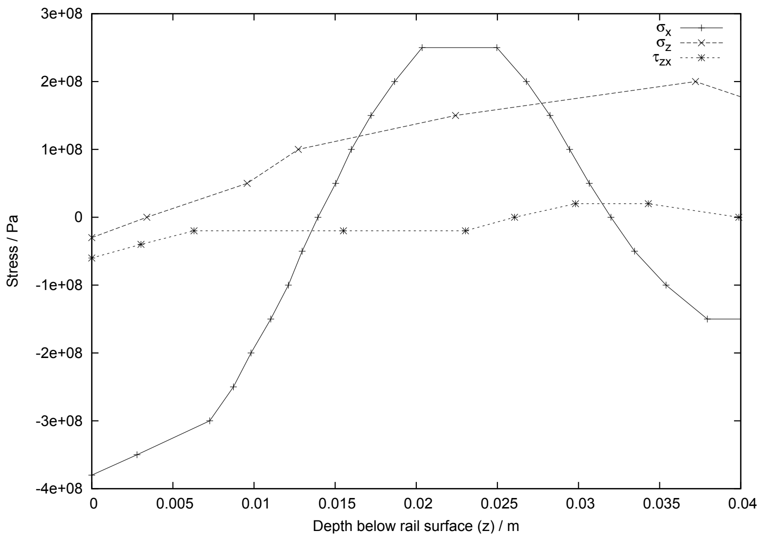

Figure 6: Input values of residual stress, varying with depth below the rail head centre. σ_x is the longitudinal stress, σ_z is the vertical stress, and τ_{zx} is the shear stress. All stress values in Pa, position values in metres.

3.2 Runs undertaken

Both the 2d (line contact) and 2.5d (elliptical contact) models were considered, both with and without each component of residual stress applied, as summarised in Table 1. All the cracks considered were taken to be at 30° below the surface. Runs were completed with both the standard shear stress values (marked + in the table), and with values reversed (marked - in the table).

For runs in which contact pressure was applied (to check the effect of residual stress alone some runs were made without the contact stress present, see below) the maximum Hertzian contact pressure of 1500MPa was chosen, simulating the mid to upper level of contact pressure found in practice [7, 8]. Surface and crack face friction coefficients were set at 0.18, representing a wet rail with water present inside surface breaking cracks [9, 10]. For elliptical cracks an ellipticity ratio (E, ratio of largest to shortest axis length) of 1.5 was chosen, giving a contact of greatest length in the direction parallel to the longitudinal axis of the rail. The area of the contact, and consequently the axis half-lengths (a and b), was related to contact pressure using Equation (4) [8]. Area is taken in mm^2 and contact pressure in MPa.

$$area = 11923 P_0^{-0.6818} = \pi ab = \pi E a^2 \tag{4}$$

3.3 Results

3.3.1 Import of residual stress

Figure 19 (Appendix A) show plots of the residual stress alone output from the modelling software. These plots are for verification only, and show that the residual stresses are correctly read and interpolated by the software.

3.3.2 Crack growth rate plots

Figures 7 and 8 summarise the results of the crack growth rate calculation runs detailed in Table 1.

Considering first the results for 2d contact (Figure 7) it is clear that the presence of residual stresses generally causes an increase in the predicted crack growth rate at all crack lengths. At crack lengths up to around 28mm (corresponding to a depth of 14mm for the 30° cracks considered here) the increase in growth rate over that for the baseline case (no residual stresses) may be classified as mild, with rates of up to 1.5 times those for the baseline case. Above 28mm in crack length the increase in growth rate can be much more dramatic (depending on which component of residual stress is considered, see below) with rates around 100 times higher than for the baseline case.

The runs conducted included the application of individual components of residual stress, as well as those with all components applied. Although such runs are somewhat artificial, they are useful in revealing which components of residual stress are most important in the changes produced in the predicted crack growth rate. From Figure 7 it can be seen that application of "positive" standard shear stress input data (i.e. without being multiplied by -1) alone has almost no effect on crack growth rate. Application of "negative" reversed shear stress or longitudinal stresses alone produces a mild increase in predicted crack growth rates. However, it is the vertical stresses in the rail which produce the most dramatic effects, and these are responsible for the very large increases in crack growth rate seen at longer crack lengths. When combinations of stresses are applied which include the vertical residual stress the results continue to show

Run no.	P_0	2d/2.5d	Long	Vertical	Shear	μ	μ_{cf}	Note
1	0	-	Y	Y	Y	-	-	Stress import check
2	1500	2d	-	-	-	0.18	0.18	Baseline run
3	1500	2.5d	-	-	-	0.18	0.18	Baseline run
4	1500	2d	Y	-	-	0.18	0.18	Rate calculation
5	1500	2.5d	Y	-	-	0.18	0.18	Rate calculation
6	1500	2d	-	Y	-	0.18	0.18	Rate calculation
7	1500	2.5d	-	Y	-	0.18	0.18	Rate calculation
8	1500	2d	-	-	+Y	0.18	0.18	Rate calculation
9	1500	2.5d	-	-	+Y	0.18	0.18	Rate calculation
10	1500	2d	-	-	-Y	0.18	0.18	Rate calculation
11	1500	2.5d	-	-	-Y	0.18	0.18	Rate calculation
12	1500	2d	Y	Y	-	0.18	0.18	Rate calculation
13	1500	2.5d	Y	Y	-	0.18	0.18	Rate calculation
14	1500	2d	Y	Y	+Y	0.18	0.18	Rate calculation
15	1500	2.5d	Y	Y	+Y	0.18	0.18	Rate calculation
16	1500	2d	Y	Y	-Y	0.18	0.18	Rate calculation
17	1500	2.5d	Y	Y	-Y	0.18	0.18	Rate calculation
18	0	2d	Y	-	-	-	-	Rate calculation
19	0	2.5d	Y	-	-	-	-	Rate calculation
20	0	2d	-	Y	-	-	-	Rate calculation
21	0	2.5d	-	Y	-	-	-	Rate calculation
22	0	2d	-	-	+Y	-	-	Rate calculation
23	0	2.5d	-	-	+Y	-	-	Rate calculation
24	0	2d	-	-	-Y	-	-	Rate calculation
25	0	2.5d	-	-	-Y	-	-	Rate calculation
26	0	2d	Y	Y	-	-	-	Rate calculation
27	0	2.5d	Y	Y	-	-	-	Rate calculation
28	0	2d	Y	Y	+Y	-	-	Rate calculation
29	0	2.5d	Y	Y	+Y	-	-	Rate calculation
30	0	2d	Y	Y	-Y	-	-	Rate calculation
31	0	2.5d	Y	Y	-Y	-	-	Rate calculation
36	1500	2d	Y	Y	+Y	0.18	-	Stress only
37	1500	2.5d	Y	Y	+Y	0.18	-	Stress only
38	1500	2d	-	-	-	0.18	-	Stress only
39	1500	2.5d	-	-	-	0.18	-	Stress only
40	1500	2d	Y	Y	+Y	0.18	0.18	Effective stress
41	1500	2.5d	Y	Y	+Y	0.18	0.18	Effective stress
42	1500	2d	-	-	-	0.18	0.18	Effective stress
43	1500	2.5d	-	-	-	0.18	0.18	Effective stress

Table 1: Conditions examined with contact stress and longitudinal, vertical and shear residual stresses. Run numbers are not sequential because some runs were not useful and are not reported. Runs were completed with both the standard shear stress values (marked + in the table), and with values reversed (marked - in the table).

very high crack growth rates at longer crack lengths irrespective of the presence of longitudinal or shear stresses.

Considering the results for 2.5d crack growth (Figure 8) the effect of residual stress can again be split into a mild effect at crack lengths below around 25mm (corresponding to a depth of around 12.5mm) and a more severe effect for lengths above this value. For the baseline case, predicted rates using the 2.5d model are generally around 20% of those predicted for the 2d model. This scaling is not reflected in the results when contact is combined with residual stresses; this is to be expected because while the region of high contact stress is confined to a smaller depth for the 2.5d case, the distribution of residual stress remains the same in both cases.

The combination of contact stress with "positive" (i.e. standard) shear stress increases the predicted crack growth rate only slightly above the baseline case. As for the 2d model, the application of "negative" (i.e. reversed) shear stress gives a much larger effect on predicted rates, but the greatest effect is again found to be from vertical residual stress. When applied alone vertical residual stress gives a crack growth rate at the longest crack lengths considered of around 40 times the baseline case. However, when applied in combination with longitudinal and shear stresses the rate drops to 20 times the baseline case. In contrast to the 2d model, rates at the longer crack lengths considered (45-60mm) have reached a plateau, and then begun to drop slightly with increasing crack length. In the 2d case rates at this stage showed rapid increases with increasing crack length.

3.3.3 Stress field plots

Figures 9 to 16 reveal which portions of a crack close to the wheel contact are open and which closed for 2d and 2.5d contact both with and without residual stress applied. For plots including residual stress, all components of residual stress were applied. These plots are useful in the interpretation of the crack growth rates predicted and plotted above. To assist in the interpretation of these figures, Figures 2 and 3 presents an example for a crack of 40mm long in a 2d stress field with residual stress applied. In all cases the plots show stress in a region ahead of and behind the contact, and can be used to find the stress along the line of a crack at 30° to the surface at any position. "Effective" stress is defined in Section 2, and takes account of crack inclination, crack face friction coefficient and crack closure. Full stress, not taking account of crack face friction and crack closure are included in Appendix B for contact stress alone, and contact stress in combination with residual stress.

3.3.4 Variation with crack length of stress intensity factors for residual stress only.

Results for the cases of residual stress alone are presented in Figures 17 and 18 (runs 18 to 31). Since residual stress alone cannot produce a stress cycle, these results are presented in terms of stress intensity factors, for use in combining the effect of residual stress with other loads such as rail bending. In the absence of a contact load the results for 2d and 2.5d contact are identical, so only the results for 2d are presented.

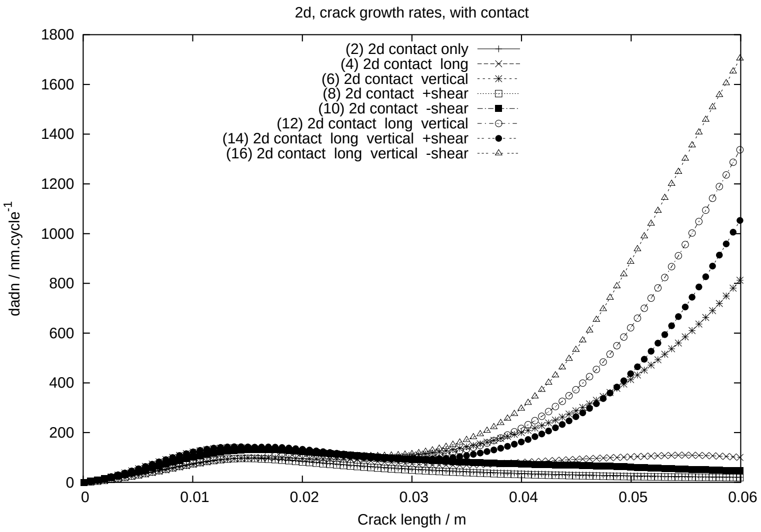

(a)

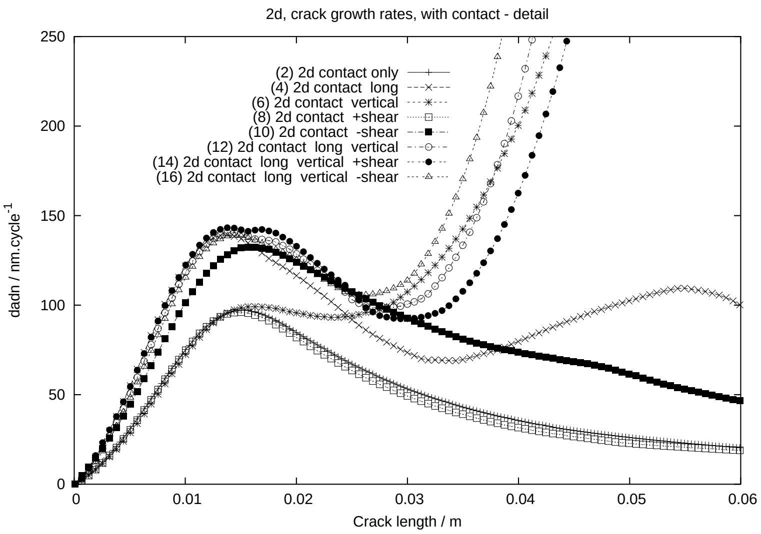

(b)

Figure 7: Summary plot of crack growth rate plotted against crack length for 2d contact. (a) Overview. (b) Detail.

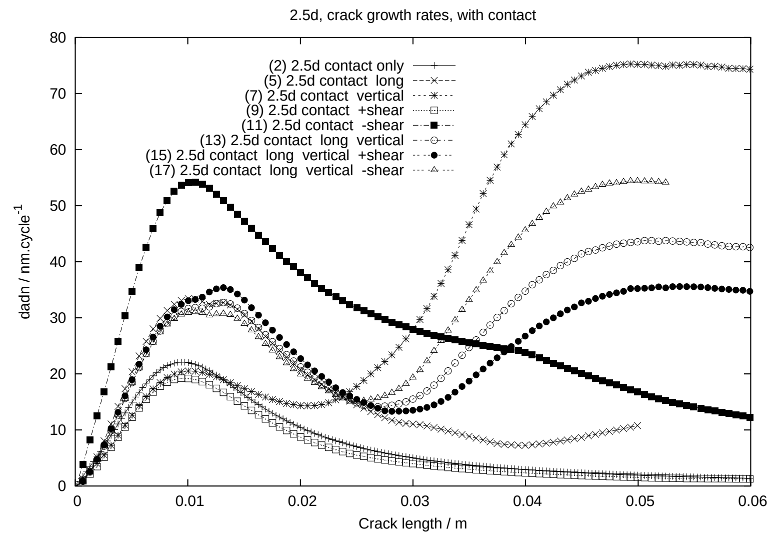

Figure 8: Summary plot of crack growth rate plotted against crack length for 2.5d contact.

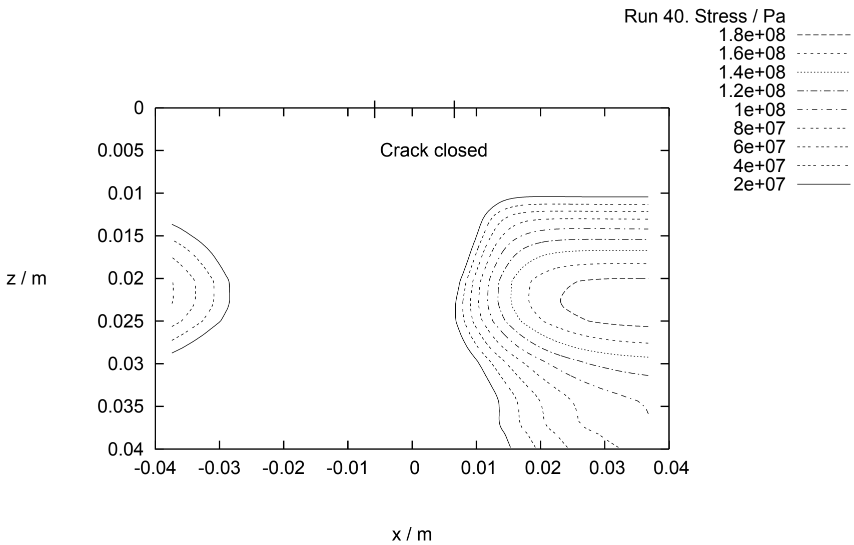

Figure 9: Run 40. Effective stress normal to a 30° crack loaded by a 2d contact and residual stress. 1500MPa Hertzian contact stress, surface and crack face friction coefficient of 0.18. Negative stresses truncated to zero, and taken to indicate crack closure. Contact indicated by vertical lines. Traction acts from right to left.

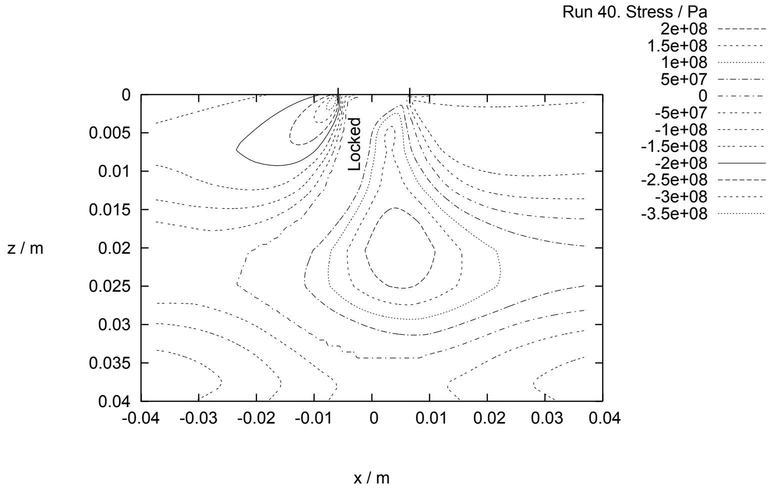

Figure 10: Run 40. Effective shear stress parallel to a 30° crack loaded by a 2d contact and residual stress. 1500MPa Hertzian contact stress, surface and crack face friction coefficient of 0.18. Shear stress is reduced by crack face friction, and set to zero where the crack is locked. Contact indicated by vertical lines. Traction acts from right to left.

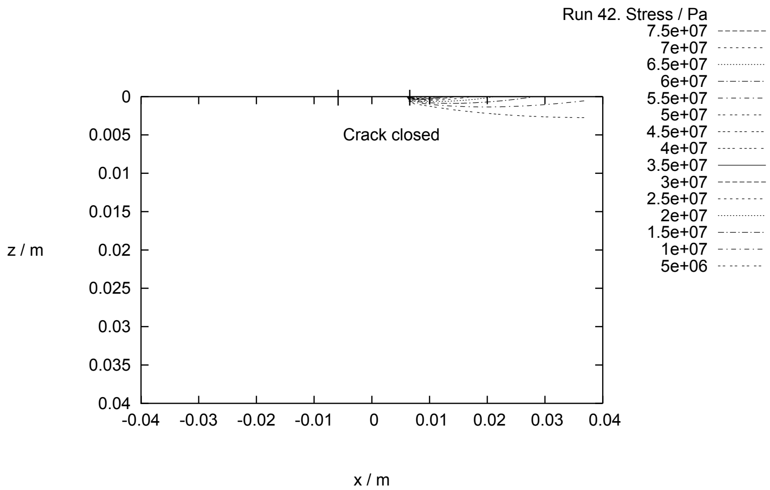

Figure 11: Run 42. Effective stress normal to a 30° crack loaded by a 2d contact. 1500MPa Hertzian contact stress, surface and crack face friction coefficient of 0.18. Negative stresses truncated to zero, and taken to indicate crack closure. Contact indicated by vertical lines. Traction acts from right to left.

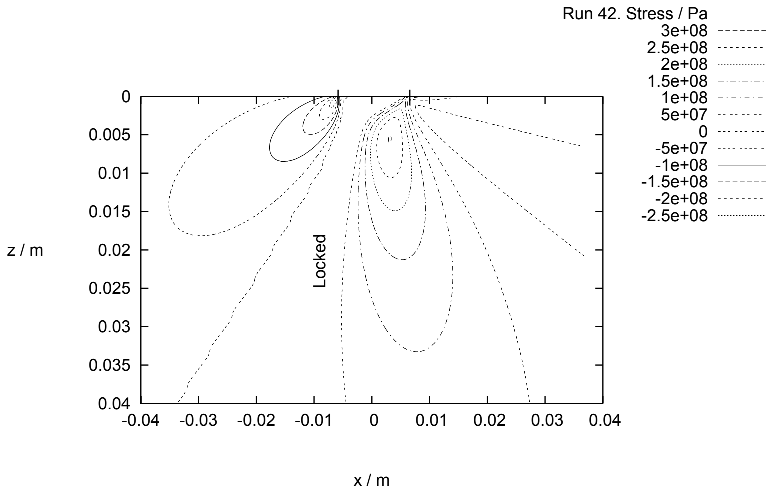

Figure 12: Run 42. Effective shear stress parallel to a 30° crack loaded by a 2d contact. 1500MPa Hertzian contact stress, surface and crack face friction coefficient of 0.18. Shear stress is reduced by crack face friction, and set to zero where the crack is locked. Contact indicated by vertical lines. Traction acts from right to left.

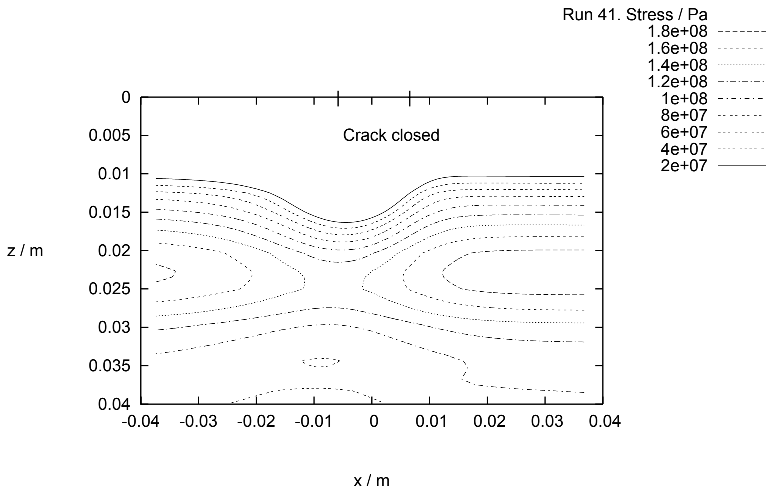

Figure 13: Run 41. Effective stress normal to a 30° crack loaded by a 2.5d contact and residual stress. 1500MPa Hertzian contact stress, surface and crack face friction coefficient of 0.18. Negative stresses truncated to zero, and taken to indicate crack closure. Contact indicated by vertical lines. Traction acts from right to left.

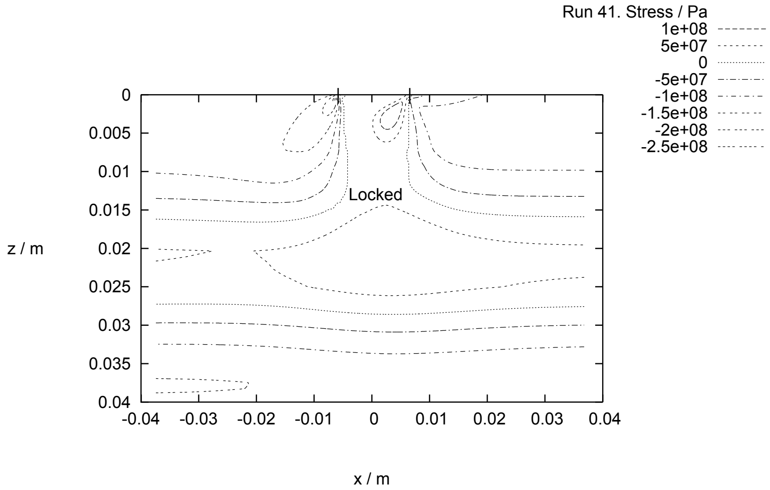

Figure 14: Run 41. Effective shear stress parallel to a 30° crack loaded by a 2.5d contact and residual stress. 1500MPa Hertzian contact stress, surface and crack face friction coefficient of 0.18. Shear stress is reduced by crack face friction, and set to zero where the crack is locked. Contact indicated by vertical lines. Traction acts from right to left.

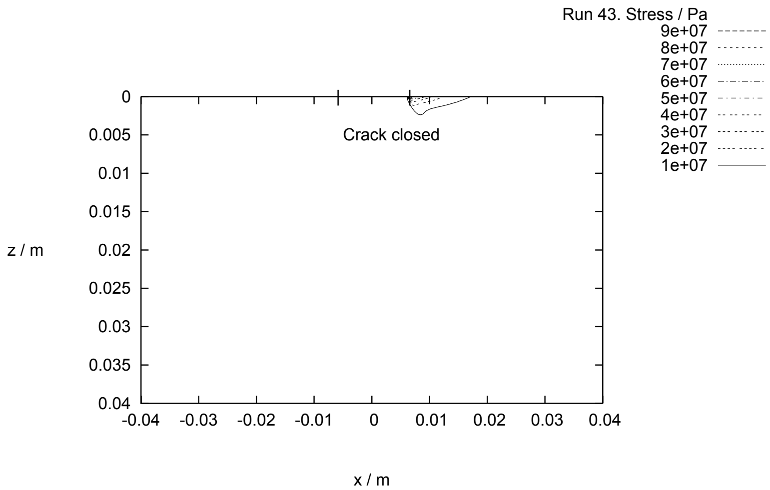

Figure 15: Run 43. Effective stress normal to a 30° crack loaded by a 2.5d contact. 1500MPa Hertzian contact stress, surface and crack face friction coefficient of 0.18. Negative stresses truncated to zero, and taken to indicate crack closure. Contact indicated by vertical lines. Traction acts from right to left.

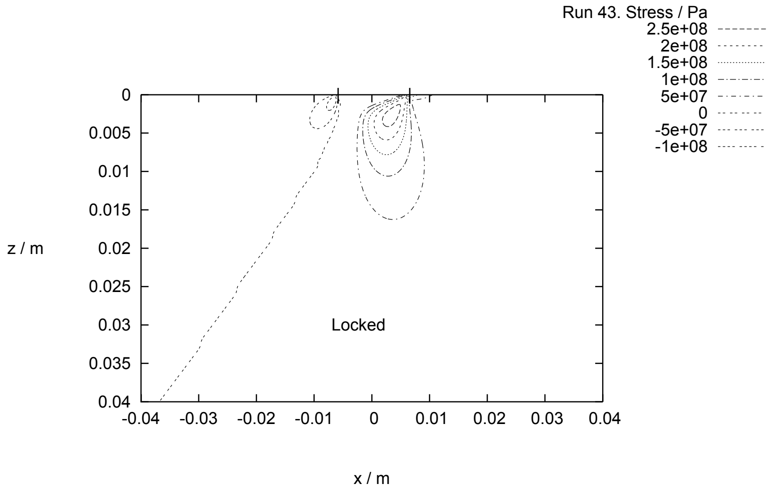

Figure 16: Run 43. Effective shear stress parallel to a 30° crack loaded by a 2.5d contact. 1500MPa Hertzian contact stress, surface and crack face friction coefficient of 0.18. Shear stress is reduced by crack face friction, and set to zero where the crack is locked. Contact indicated by vertical lines. Traction acts from right to left.

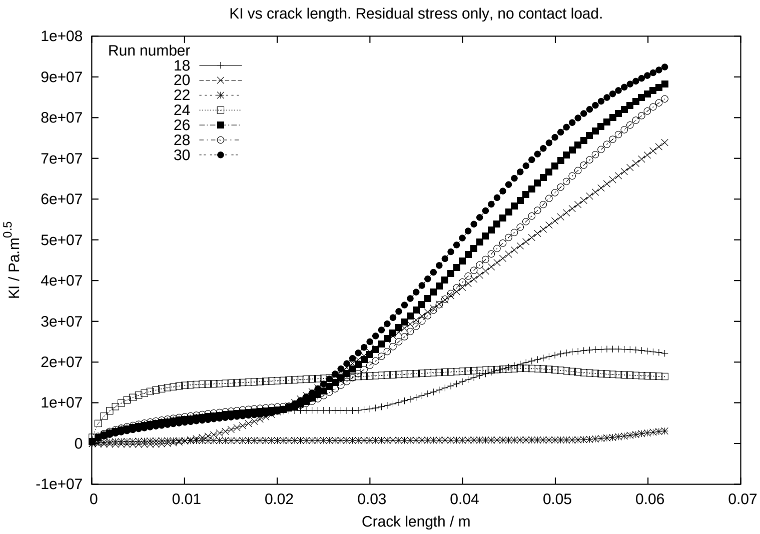

Figure 17: Variation with crack length of mode I (tensile) stress intensity factor for a crack at 30° below the rail surface. Residual stress only applied, no contact load. Run numbers are described in Table 1

3.4 Discussion

3.4.1 2d crack growth

Considering 2d contact, the application of residual stress produces a dramatic increase in the predicted crack growth rate. Comparing Figures 9 and 11 for stress resolved normal to the crack in cases with and without residual stress it can be seen that inclusion of residual stress both moves and enlarges the regions over which a crack will be open as a contact passes over it. Without residual stress, the crack is open only in a small region near to the contact surface. This indicates that as the crack grows deeper it will be closed, and any shear mode growth will be restricted. With the addition of residual stress the crack is closed when it is near the surface, but as it grows deeper and longer, increasing proportions of it will be open. When the crack is open, not only does the opening contribute to overall crack growth, but shear mode growth is unrestricted by contact between the crack faces.

Shear stress parallel to the crack for the 2d contact case is plotted in Figures 10 and 12, again including and excluding residual stresses respectively. The effect of crack closure, discussed above, is effectively included in the shear stress output, since crack locking and the degree to which sliding is limited by friction depends on the extent of closed regions along the crack, and the stress with which they are held closed. Comparing the plots it can be seen that the addition of residual stress to the stress field has reduced the area over when the crack is locked (zero effective shear stress) for the crack face friction coefficient considered. More importantly, whereas the shear stress continuously diminishes with increasing distance from the contact at depths over around 10mm in the absence of residual stress, the addition of residual stress to the contact stresses gives regions of increasing shear stress magnitude as depth increases. A particularly high peak in shear stress is present at around 20mm below the centre of the contact, although the maximum shear stress present is below that for the 2d contact without residual stress.

3.4.2 2.5d crack growth

There are many similarities between the 2d and 2.5d contact situations, although the crack growth rates at longer crack lengths are not increased as dramatically in the 2.5d case as they were in the 2d case. Through comparison of the stress fields present in the two cases, these differences in crack growth rates predicted for the two cases can be explained.

Figures 13 and 15 illustrate stresses resolved normal to the crack for cases with and without residual stresses respectively. As in the 2d case, crack closure is much reduced by the addition of residual stresses to the contact stresses, but while some deep cracks could remain closed at their tips in the 2d case, for 2.5d the closure is prevented completely at crack lengths over around 30mm. This crack length is close to the length at which "severe" acceleration of crack growth was identified in Figure 8.

Figures 14 and 16 illustrate shear stresses resolved parallel to the cracks, with and without residual stresses respectively. As for the 2d contact case shear stress tends to increase rather than decrease in magnitude with depth below about 30mm, whereas it diminishes to zero in the case without residual stress. The main difference between the 2d and 2.5d cases with residual stress is the absence in the 2.5d case of the high peak in shear stress at a depth of around 20mm. This reflects the concentration of shear stress nearer to the surface in the 2.5d case relative to the 2d case, and is thought to be the key to the differences between the predicted crack growth rates for the two models.

Although the deepest stresses illustrated (at around 40mm deep) are similar for both 2d and 2.5d cases, the high stress peak at 20mm below the contact is only present in the 2d case. High shear stresses along the length of cracks are crucial in determining the mode II stress intensity factor (and hence crack growth rate) and although stress at the tip are the most highly weighted in SIF calculation, those further back remain significant. This "weighting" in the effect of stress at different points along the crack is illustrated in Figure 1b which shows the Green's functions for calculation of mode II SIF for a crack loading in shear.

3.5 Conclusions

Calculations to predict the effect of residual stress on crack growth in rails have shown that residual stresses can dramatically increase the predicted crack growth rates. The effect is most important at long crack lengths, where the contact stresses have diminished to much lower levels than at the surface. Modelling using 2d and 3d (through the 2.5d model) contact stress fields has been carried out, and differences revealed between the predicted effect of residual stress on crack growth rates. It is thought that the 2.5d model is the more realistic of these models because it more closely approximates the rail-wheel contact. Validation of the results through experiments or track tests would be useful to check the capabilities of the models.

The residual stress calculations reported here have highlighted the importance of the vertical component of residual stress in determining crack growth rate. Unfortunately, most existing data on residual stresses concentrates on longitudinal stresses. In the collection of residual stress data within the project it will be important to measure vertical residual stresses. This will allow further calculations to be conducted using alternative residual stress data to examine the sensitivity of the findings to the specific data used.

The relative importance of vertical and longitudinal residual stresses will almost certainly be a function of the crack inclination angle. All the calculations so far have been for a crack at 30° below the rail surface. Further angles should be considered, particularly to investigate the effect of residual stress on cracks which have turned down into the rail.

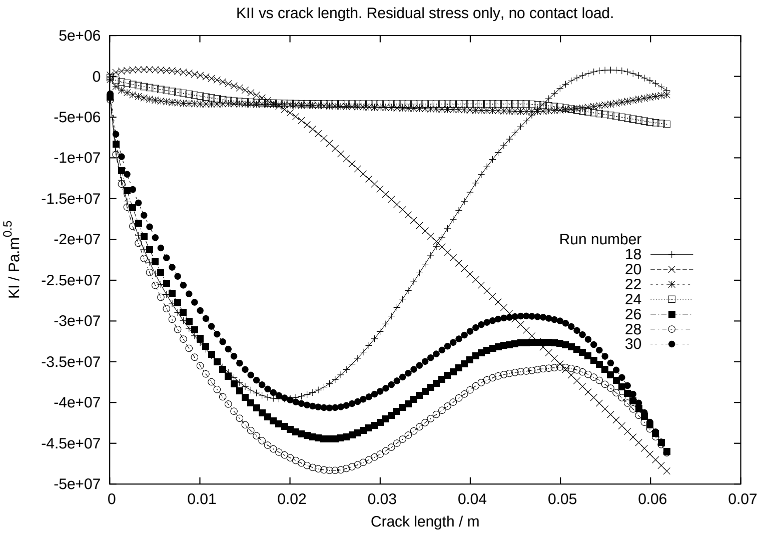

Figure 18: Variation with crack length of mode II (shear) stress intensity factor for a crack at 30° below the rail surface. Residual stress only applied, no contact load. Run numbers are described in Table 1

References

[1] D I Fletcher and J H Beynon. A simple method of stress intensity factor calculation for inclined surface breaking cracks with crack face friction under contact loading. *Proceedings of the Institution of Mechanical Engineering Part J, Journal of Engineering Tribology*, 213:481–486, 1999.

[2] D P Rooke, D B Rayaprolu, and M H Aliabadi. Crack line and edge green's functions for stress intensity factors of inclined edge cracks. *Fatigue and Fracture of Engineering Materials and Structures*, 15(5):441–461, 1992.

[3] M Kaneta, H Yatsuzuka, and Y Murakami. Mechanism of crack growth in lubricated rolling/sliding contact. *ASLE Transactions*, 28(3):407–414, 1985.

[4] A Kapoor, D I Fletcher, F J Franklin, and F Alwahdi. Whole life rail model, interim report. Technical Report MEC/AK/AEAT/September02/, The University of Sheffield and AEAT, 2002.

[5] P E Bold, M W Brown, and R J Allan. Shear mode crack growth and rolling contact fatigue. *Wear*, 144:307–317, 1991.

[6] A Kapoor and D I Fletcher. Post Hatfield rolling contact fatigue. The effect of residual stress on contact stress driven crack growth in rail. Literature review. Technical Report WR061106-1, Newcastle University, November 2006.

[7] J Kalousek. Wear and contact fatigue model for railway rail. Technical Report 1986/10, National Research Council Canada, 1986.

[8] A Kapoor and D I Fletcher. Whole life rail model, stage 1 final report. Technical Report MEC/AK/AEAT/June01/, The University of Sheffield and AEAT, 2001.

[9] D I Fletcher and J H Beynon. Equilibrium of crack growth and wear rates during unlubricated rolling-sliding contact of pearlitic rail steel. *Proceedings of the Institution of Mechanical Engineering Part F, Journal of Rail and Rapid Transit*, 214:93–105, 2000.

[10] W R Tyfour, J H Beynon, and A Kapoor. Deterioration of the rolling contact fatigue life of pearlitic rail steel due to dry-wet rolling-sliding line contact. *Wear*, 197:255–265, 1996.

A Verification of residual stress import.

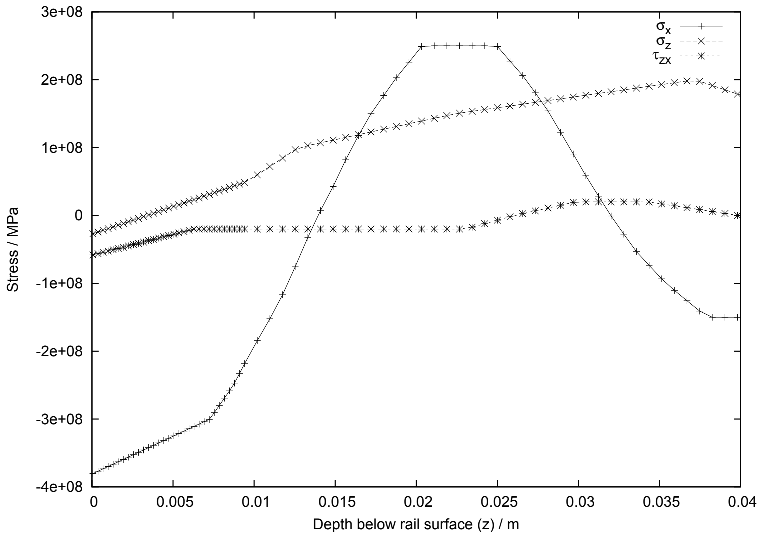

Figure 19: Output from modelling software to validate variation with depth of residual stress. To be compared with Figure 6. σ_x is the longitudinal stress, σ_z is the vertical stress, and τ_{zx} is the shear stress. All stress values in Pa, position values in metres.

B Contour plots of sub-surface stresses, resolved along the crack line

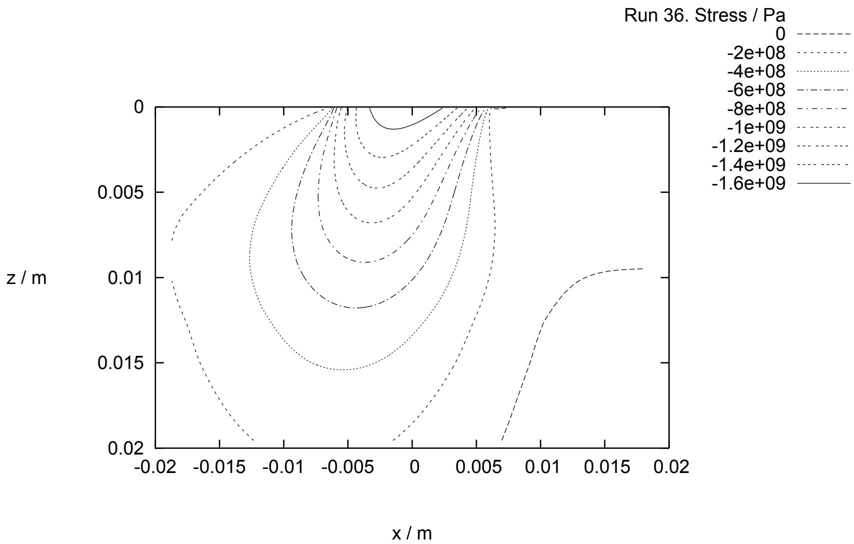

Figure 20: Run 36. Stress normal to a 30° crack loaded by a 2d contact and residual stress. 1500MPa Hertzian contact stress, surface and crack face friction coefficient of 0.18. Traction acts from right to left.

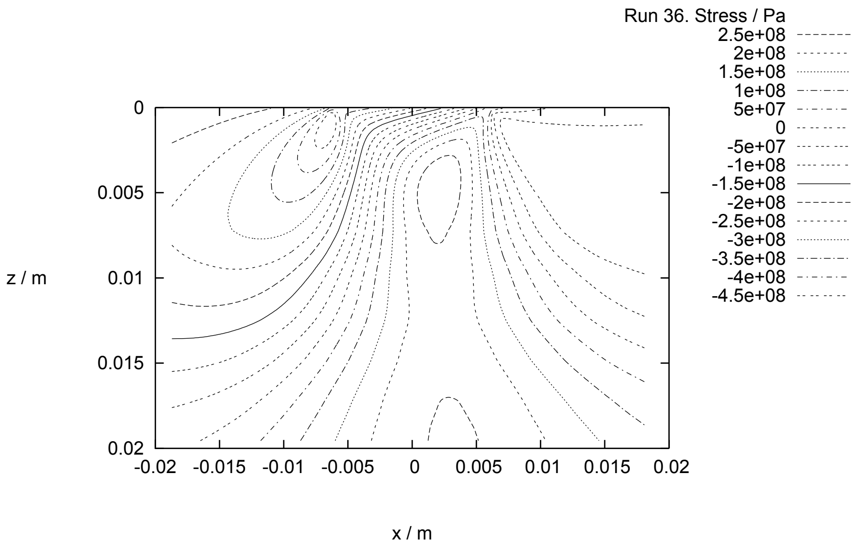

Figure 21: Run 36. Shear stress parallel to a 30° crack loaded by a 2d contact and residual stress. 1500MPa Hertzian contact stress, surface and crack face friction coefficient of 0.18. Traction acts from right to left.

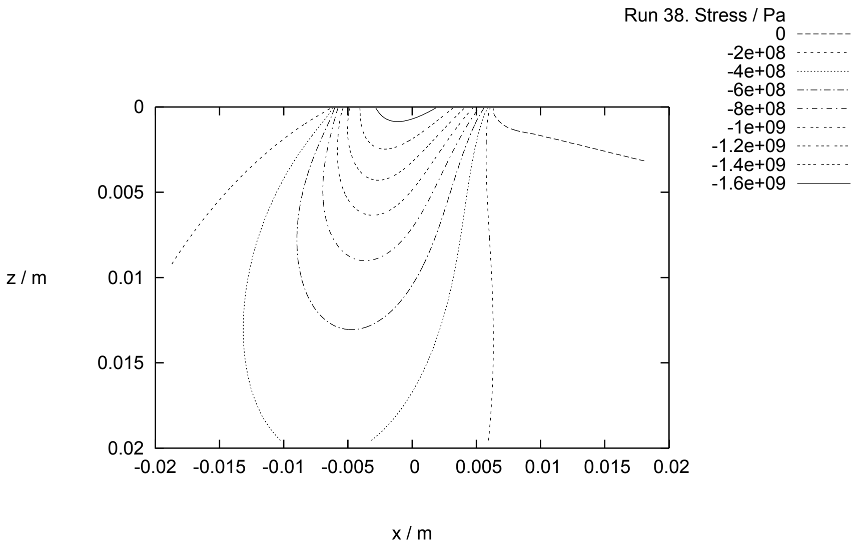

Figure 22: Run 38. Stress normal to a 30° crack loaded by a 2d contact. 1500MPa Hertzian contact stress, surface and crack face friction coefficient of 0.18. Traction acts from right to left.

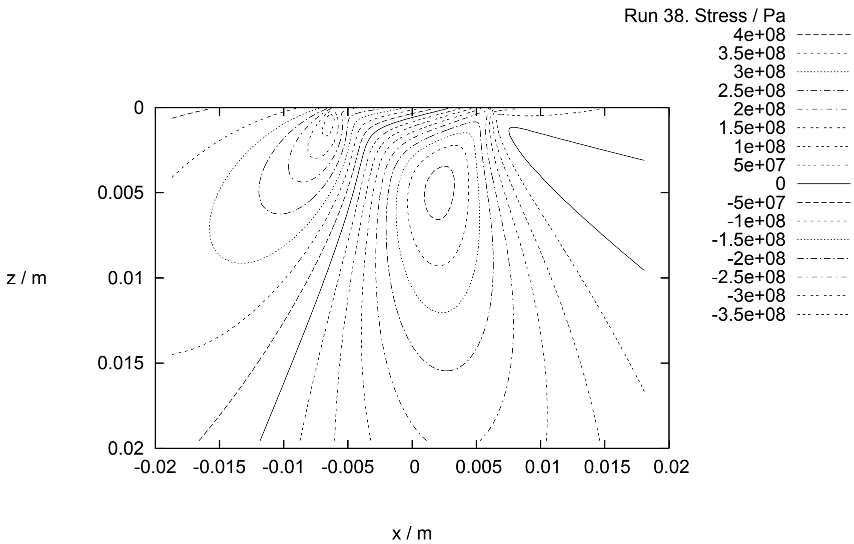

Figure 23: Run 38. Shear stress parallel to a 30° crack loaded by a 2d contact. 1500MPa Hertzian contact stress, surface and crack face friction coefficient of 0.18. Traction acts from right to left.

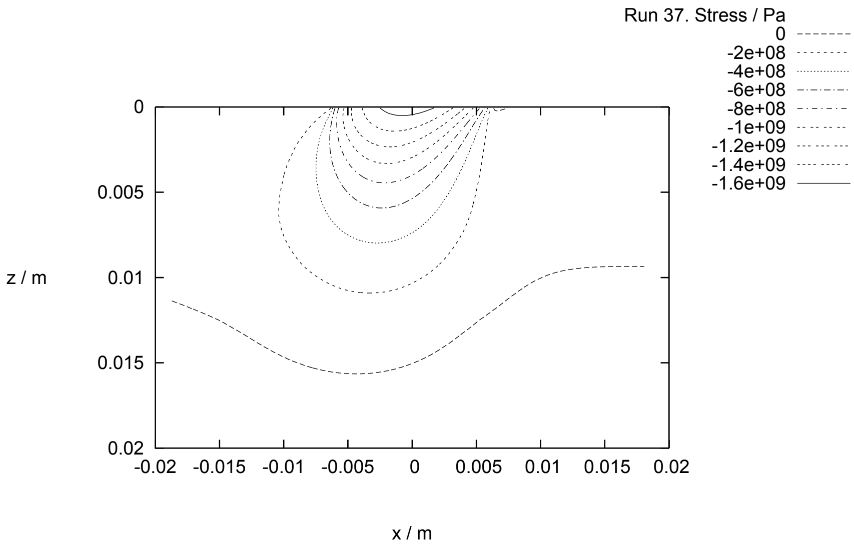

Figure 24: Run 37. Stress normal to a 30° crack loaded by a 2.5d contact and residual stress. 1500MPa Hertzian contact stress, surface and crack face friction coefficient of 0.18. Traction acts from right to left.

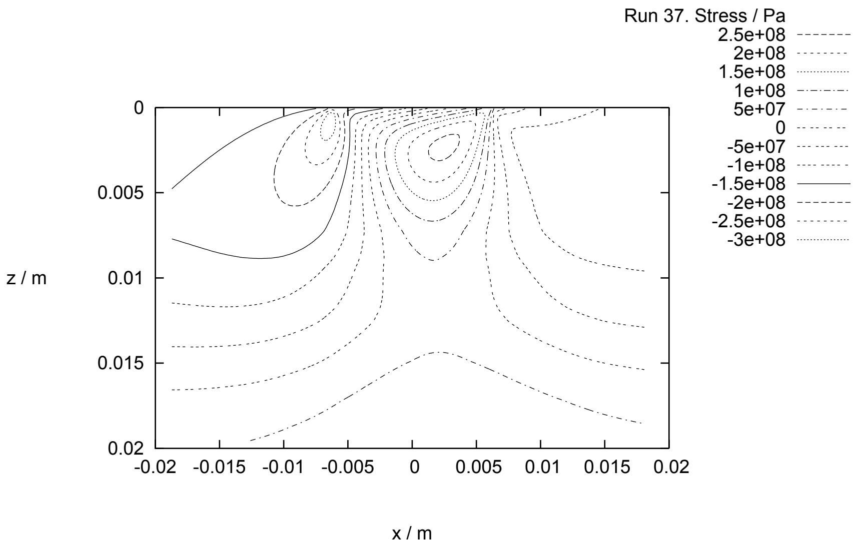

Figure 25: Run 37. Shear stress parallel to a 30° crack loaded by a 2.5d contact and residual stress. 1500MPa Hertzian contact stress, surface and crack face friction coefficient of 0.18. Traction acts from right to left.

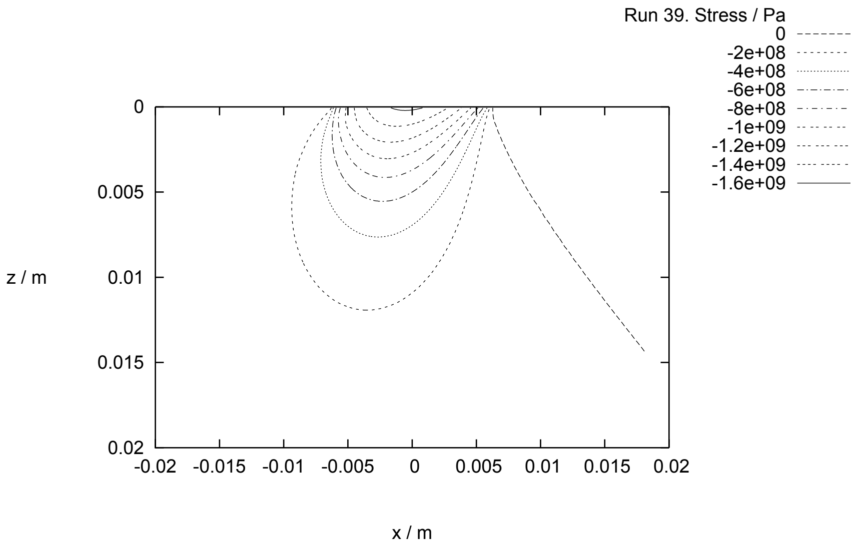

Figure 26: Run 39. Stress normal to a 30° crack loaded by a 2.5d contact. 1500MPa Hertzian contact stress, surface and crack face friction coefficient of 0.18. Traction acts from right to left.

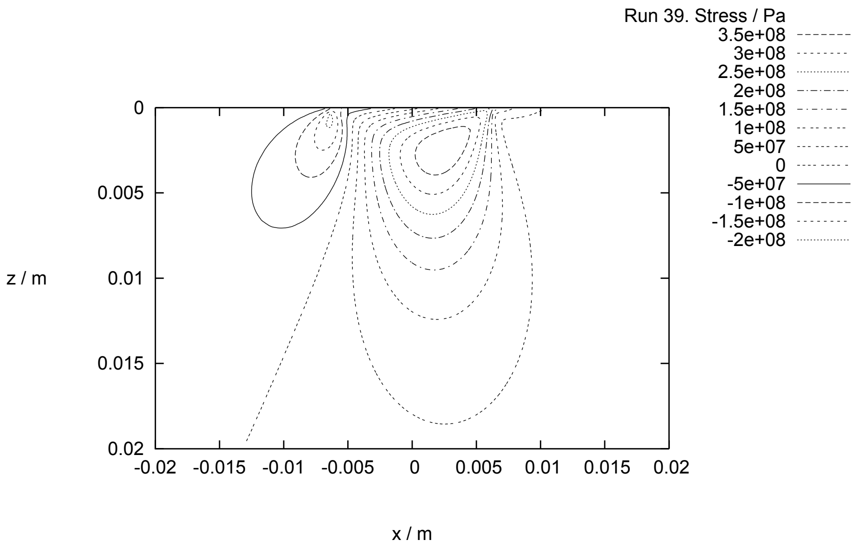

Figure 27: Run 39. Shear stress parallel to a 30° crack loaded by a 2.5d contact. 1500MPa Hertzian contact stress, surface and crack face friction coefficient of 0.18. Traction acts from right to left.